First-principles study of the angular dependence of the spin-orbit torque in Pt/Co and Pd/Co bilayers

Farzad Mahfouzi* and Nicholas Kioussis†
Department of Physics and Astronomy, California State University, Northridge, California 91330, USA

(Received 16 April 2018; published 25 June 2018)

Spin-orbit torque (SOT) induced by spin Hall and interfacial effects in heavy-metal (HM)/ferromagnetic (FM) bilayers has recently been employed to switch the magnetization direction using in-plane current injection. In this paper, using the Keldysh Green's function approach and first-principles electronic structure calculations we determine the fieldlike (FL) and dampinglike (DL) components of the SOT for the HM/Co (HM = Pt,Pd) bilayers. Our approach yields the angular dependence of both the FL- and DL-SOT on the magnetization direction without assuming *a priori* their angular form. Decomposition of the SOT into the Fermi sea and Fermi surface contributions reveals that the SOT is dominated by the latter. Due to the large lattice mismatch between the Co and the HM we have also determined the effect of tensile biaxial strain on both the FL- and DL-SOT components. The calculated dependence of FL- and DL-SOT on the HM thickness is overall in good agreement with experiment. The dependence of the SOT with the position of the Fermi level suggests that the DL-SOT is dominated by the spin Hall effect of the bulk HM.

DOI: 10.1103/PhysRevB.97.224426

I. INTRODUCTION

Spin-orbit torque (SOT) due to in-plane current flow in heavy-metal/ferromagnet (HM/FM) bilayers has attracted considerable attention in recent years as a method to switch efficiently the magnetization direction of ultrathin FM films at room temperature [1–7]. Experimental [2,5,7,8] and theoretical [9–11] studies have established that the SOT can be separated into fieldlike (FL), $T^{\mathrm{FL}}\vec{m}\times\vec{y}$, and dampinglike (DL), $T^{\mathrm{DL}}\vec{m}\times(\vec{m}\times\vec{y})$, components, where $\vec{m}$ is the unit vector pointing along the direction of the magnetization and $\vec{y}$ is an in-plane unit vector normal to the applied electric field. In the linear response regime, the FL-SOT affects both the size and direction of the effective magnetic field exerted on the magnetic moment, while the DL-SOT only reorients the effective field and is responsible for the angular momentum transfer between the flowing electrons and the FM, thus modulating the ferromagnetic resonance linewidth of the FM [12–14].

Experimentally, different techniques, including the adiabatic (low-frequency) harmonic Hall voltage [15–18], the spin-torque ferromagnetic resonance (ST-FMR) [18–22], and the magneto-optical Kerr effect (MOKE) [23,24], have been used to quantitatively measure the DL- and FL-SOT components. Furthermore, the adiabatic harmonic Hall voltage approach has been recently employed to investigate the magnetization orientation dependence of the SOT [17,25,26].

The experimental observations invite several important questions pertaining to the microscopic origin of (i) the bulk versus interfacial SOT [9,11,27,28], (ii) higher-order angular terms of the FL-SOT [8,17,25,26], and (iii) the HM thickness dependence of the SOT [17,29]. To address these questions an accurate description of the electronic structure of the bilayer in terms of the crystal structure and the interfacial hybridization of the electron orbitals is necessary, signifying the importance of the first-principles study of the SOT phenomena [11,30].

The objective of this work is to employ an *ab initio*-based framework which links the Keldysh Green's function approach with first-principles electronic structure calculations to determine the FL- and DL-SOT of the Co/Pt and Co/Pd (111) bilayers. This approach yields the well-known angular forms for both SOT components without assuming *a priori* their angular dependence. We show that the DL-SOT can be separated into Fermi sea and Fermi surface contributions where the latter is dominant. We present results of the effect of biaxial strain and of heavy-metal thickness on both components of the SOT, and compare the *ab initio* results with experiment. In agreement with experiment, we find that the FL-SOT extrapolates to a nonzero value with decreasing the HM thickness, indicating its interfacial origin due the Rashba-Edelstein effect (REE). On the other hand, the DL-SOT vanishes with decreasing HM thickness, suggesting its bulk origin due to the spin Hall effect (SHE). This is corroborated by the strong correlation of the dependence of the DL-SOT and spin Hall conductivity (SHC) on the Fermi level position of the heavy metal.

II. THEORETICAL FORMALISM

The magnetization dynamics of a FM described by a time-dependent unit vector $\vec{m}$ along the magnetization orientation, is described by the Landau-Lifshitz-Gilbert (LLG) equation of motion,

$$\frac{d\vec{m}}{dt} = -\vec{m}\times\gamma\vec{H}_{\mathrm{ext}} + \vec{T} + \alpha\vec{m}\times\frac{d\vec{m}}{dt}. \tag{1}$$

*Farzad.Mahfouzi@gmail.com
†Nick.Kioussis@csun.edu

Here, γ is the gyromagnetic ratio, α is the Gilbert damping constant, $\vec{H}_{\rm ext}$ is the external magnetic field, and $\vec{T}$ is the current-induced torque on the FM which can be written in the form

$$\vec{T} = \frac{1}{N_k M_s}\vec{m} \times \sum_{\vec{k}} \mathrm{Tr}\left(\frac{\partial \hat{H}_{\vec{k}}}{\partial \vec{m}}\hat{\rho}_{\vec{k}}\right), \tag{2}$$

where N_k is the number of the k-point mesh for the numerical integration, M_s is the magnetic moment per unit cell in units of Bohr magneton μ_B, $\hat{H}_{\vec{k}}(\vec{m})$ is the electronic Hamiltonian which depends on $\vec{m}$, and $\hat{\rho}_{\vec{k}}$ is the electronic density matrix.

In the absence of an external electric field or a time-dependent term in the Hamiltonian, the electronic density matrix is given by $\hat{\rho}^{\rm eq}_{\vec{k}} = \int dE\, \mathrm{Im}(\hat{G}_{\vec{k}E}) f(E)/\pi$, where $\hat{G}_{\vec{k}E} = (E - i\eta - \hat{H}_{\vec{k}})^{-1}$ is the electron Green's function and $f(E)$ is the Fermi distribution function. Here, $\eta = \hbar/2\tau$ is the broadening parameter, where τ is the relaxation time for the excited electrons. Typically, $\vec{T}^{\rm eq}$ contributes to the exchange interaction between local moments and is responsible for the magnetocrystalline anisotropy arising from the spin-orbit coupling (SOC). To go beyond the equilibrium regime and investigate the effect of the external electric field on the density matrix, we employ the Keldysh Green's function formalism [31], where the density matrix is given by $\hat{\rho}_{\vec{k}} = \eta \int dE \hat{G}_{\vec{k}E} f(E) \hat{G}^{\dagger}_{\vec{k}E}/\pi$. In the presence of an external electric field $\vec{E}_{\rm ext}$, the resulting linear drop in the chemical potential, $\delta\mu(\vec{x}) = e\vec{E}_{\rm ext}\cdot\vec{x}$, can be taken into account by replacing the energy in the integrand with $E \to E + ie\vec{E}_{\rm ext}\cdot\vec{\nabla}_{\vec{k}}$, where we ignore the chemical potential drop inside each unit cell, and use $\vec{x} = i\vec{\nabla}_{\vec{k}}$ for the position operator. In the linear response regime the nonequilibrium density matrix of the electrons under an external electric field along the x direction is

$$\frac{\hat{\rho}^{\rm neq}_{\vec{k}}}{eE^x_{\rm ext}} = \hbar \int \frac{dE}{2\pi i}\Bigg[\mathrm{Im}\left(\hat{G}_{\vec{k}E}\frac{\partial \hat{G}_{\vec{k}E}}{\partial k_x} - \frac{\partial \hat{G}_{\vec{k}E}}{\partial k_x}\hat{G}_{\vec{k}E}\right) f(E) - \eta\left(\hat{G}_{\vec{k}E}\frac{\partial \hat{G}^{\dagger}_{\vec{k}E}}{\partial k_x} - \frac{\partial \hat{G}_{\vec{k}E}}{\partial k_x}\hat{G}^{\dagger}_{\vec{k}E}\right)\frac{\partial f(E)}{\partial E}\Bigg]. \tag{3}$$

The first term in the integrand is the Fermi sea contribution originating from the modification of the single-electron Green's function due to the electric field and the second term is the Fermi surface contribution. Using the Fermi surface (FS) contribution of the nonequilibrium density matrix in Eq. (2), the FS contribution to the current-induced SOT torkance $\vec{\tau}_{\rm FS} = \vec{T}^{\rm neq}_{\rm FS}/eE^x_{\rm ext}$ is given by

$$\vec{\tau}_{\rm FS} = \frac{1}{\pi M_s N_k}\vec{m} \times \sum_{\vec{k}} \mathrm{Im}\left(\mathrm{Tr}\left[\frac{\partial \hat{H}_{\vec{k}}}{\partial \vec{m}}\mathrm{Im}(\hat{G}_{\vec{k}})\hat{v}^{k_x}\hat{G}_{\vec{k}}\right]\right). \tag{4}$$

Here, $\hat{v}^{k_x} = \frac{\partial \hat{H}_{\vec{k}}}{\partial k_x}$ is the group velocity matrix and the Green's functions are calculated at the Fermi energy $E = E_F$. The torkance can be separated into the fieldlike ($\vec{\tau}^{\rm FL}$) and a dampinglike ($\vec{\tau}^{\rm DL}$) components corresponding to the imaginary and real parts of the Green's function, $\hat{G}_{\vec{k}} = \mathrm{Re}(\hat{G}_{\vec{k}}) + i\,\mathrm{Im}(\hat{G}_{\vec{k}})$, respectively. Note that $\vec{\tau}^{\rm FL}$ ($\vec{\tau}^{\rm DL}$) is even (odd) under $\eta \to -\eta$ transformation. A similar decomposition can also be made from the even and odd components of the torkance under $\vec{m} \to -\vec{m}$ transformation [11].

The total nonequilibrium density matrix given by Eq. (3) can be rewritten in the following form,

$$\frac{\hat{\rho}^{\rm neq}_{\vec{k}}}{eE^x_{\rm ext}} = \hbar \int \frac{dE}{\pi}\Bigg[\mathrm{Im}(\hat{G}_{\vec{k}E})\hat{v}_{k_x}\,\mathrm{Im}(\hat{G}_{\vec{k}E})\frac{\partial f(E)}{\partial E} - 2\,\mathrm{Im}\big[\mathrm{Im}(\hat{G}_{\vec{k}E})\hat{v}_{k_x}\,\mathrm{Re}\big(\hat{G}^2_{\vec{k}E}\big)\big] f(E)\Bigg], \tag{5}$$

where the first term leads to the FL-SOT and remains to be a FS quantity only, $\tau^{\rm FL}_{\rm tot} = \tau^{\rm FL}_{\rm FS}$. The second term leads to the total DL-SOT, where, in the ballistic regime, $\eta \to 0$, and in a representation in which the Hamiltonian is diagonal, we can use $\mathrm{Im}(\hat{G}_{\vec{k}E})_{nn} = \pi\delta(E - \varepsilon_n(\vec{k}))$ to obtain

$$\vec{\tau}^{\rm DL}_{\rm tot} = \frac{2}{M_s N_k}\vec{m} \times \sum_{nm\vec{k}} \mathrm{Re}\left(\frac{\mathrm{Im}\big[\big(\frac{\partial \hat{H}_{\vec{k}}}{\partial \vec{m}}\big)_{nm}\hat{v}^{k_x}_{mn}\big]}{(\varepsilon_{n\vec{k}} - \varepsilon_{m\vec{k}} - i\eta)^2}\right) f(\varepsilon_{n\vec{k}}), \tag{6}$$

where n and m are band indices and $\varepsilon_{n\vec{k}}$ are the energy bands. Equation (6) is sometimes rewritten in terms of the Berry curvature [10,11,32]. Note that in contrast to the Fermi surface contribution to the SOT in Eq. (4), Eq. (6) yields a nonzero DL-SOT even for a vanishing density of states at the Fermi energy [$\mathrm{Im}(G_{\vec{k}E_F})$], as in the case of ferromagnetic/topological insulator (TI) heterostructures, where the proximity-induced exchange splitting at the interface can open a gap on the surface state of the TI [27,33,34]. In Sec. IV we present results for both Fermi sea and Fermi surface contributions to the DL-SOT using Eqs. (4) and (6), respectively.

III. DFT CALCULATION

The density functional theory (DFT) calculations for the hcp Co(0001)/fcc Pt(111) and Co(0001)/fcc Pd(111) bilayers were carried out using the Vienna *ab initio* simulation package (VASP) [35,36]. The pseudopotential and wave functions are treated within the projector augmented-wave (PAW) method [37,38]. Structural relaxations were carried using the generalized gradient approximation as parametrized by Perdew *et al.* [39] when the largest atomic force is smaller than 0.01 eV/Å. As illustrated in Fig. 1(b), the HM(m)/Co(n) bilayer is modeled employing the slab supercell approach along the [111] consisting of m fcc Pt or Pd monolayers (MLs) with ABC stacking ($m = 1,2,\ldots,8$) and $n = 6$ hcp Co MLs with AB stacking. A 25-Å-thick vacuum region is introduced to separate the periodic slabs along the stacking direction (i.e., z axis). The plane-wave cutoff energy is 500 eV and a $14\times14\times1$ k-point mesh is used in the two-dimensional (2D) Brillouin zone (BZ) sampling. The in-plane lattice constant of the hexagonal unit cell is set to the experimental value of 2.505 Å for bulk Co. Furthermore, in order to investigate the effect of epitaxial strain on the SOT, we have varied the in-plane lattice constant in the range of $a \in (2.5, 2.77)$ Å, where the latter value corresponds to the bulk Pt lattice constant. Using the tight-binding (TB) Hamiltonian obtained from the VASP-WANNIER90 calculations [40], we have calculated the SOT versus magnetization orientation with a $500\times500\times1$ k-point mesh for the BZ sampling [41]. In this approach, the TB Hamiltonian was

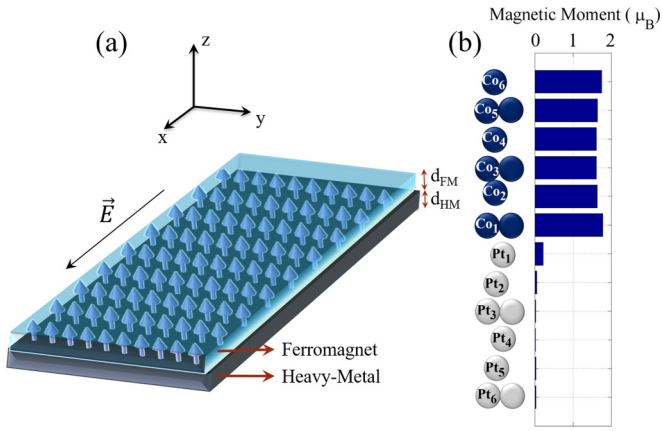

FIG. 1. (a) Schematic device setup consisting of a ferromagnet/heavy-metal bilayer system under an applied electric field along the x axis. (b) Atomic stacking along the [111] direction of the Co/Pt bilayer slab composed of six layers of hcp Co on six layers of fcc Pt(111). We also show the layer-resolved magnetic moment.

calculated using the tight-binding parameters obtained from VASP-WANNIER90 calculations [40]. The electron Hamiltonian matrix in momentum space $\vec{k}$ and localized atomic orbital basis sets is given by $\hat{H}_{\vec{k}} = \hat{H}^0_{\vec{k}} \otimes \hat{1}_{2\times 2} + \hat{\Delta}_{\vec{k}} \otimes \vec{m}\cdot\hat{\vec{\sigma}}$, where $\otimes$ represents the direct product, $\hat{\vec{\sigma}}$'s are the Pauli matrices, and the non-spin-polarized term $\hat{H}^0_{\vec{k}}$ and the exchange splitting term $\hat{\Delta}_{\vec{k}}$ are calculated within the Wannier basis from

$$\hat{H}^0_{\vec{k}} = \hat{H}_{\rm SOC} + \frac{1}{2}\sum_{\vec{n}}\frac{1}{D_{\vec{n}}}(\hat{H}^{\uparrow\uparrow}_{\vec{n}} + \hat{H}^{\downarrow\downarrow}_{\vec{n}})e^{i\sum_j n_j \vec{a}_j\cdot\vec{k}}, \quad (7)$$

$$\hat{\Delta}_{\vec{k}} = \frac{1}{2}\sum_{\vec{n}}\frac{1}{D_{\vec{n}}}(\hat{H}^{\uparrow\uparrow}_{\vec{n}} - \hat{H}^{\downarrow\downarrow}_{\vec{n}})e^{i\sum_j n_j \vec{a}_j\cdot\vec{k}}, \quad (8)$$

where $\hat{H}_{\rm SOC}$ is the SOC Hamiltonian matrix, $\hat{H}^{\uparrow\uparrow}_{\vec{n}}$ and $\hat{H}^{\downarrow\downarrow}_{\vec{n}}$ are the spin-majority and spin-minority matrices, $\vec{a}_j$'s are the primitive lattice vectors, $\vec{n} = (n_1, n_2, n_3)$ are integers denoting the lattice positions, and $D_{\vec{n}}$ is the degeneracy of the Wigner-Seitz grid point.

The $\hat{H}^{\uparrow\uparrow}_{\vec{n}}$ and $\hat{H}^{\downarrow\downarrow}_{\vec{n}}$ are determined from spin-polarized VASP-WANNIER90 calculations without SOC in an $|I, lms\rangle$ basis set, where I corresponds to the ionic index, lm represent the spherical harmonic indices, and s corresponds to the spin index. The SOC Hamiltonian is constructed using

$$\langle I, lms|\hat{H}_{\rm SOC}|I', l'm's'\rangle = \frac{1}{2}\delta_{ll'}\delta_{II'}\xi^I_l \sum_i \langle lm|\hat{L}_i|lm'\rangle\hat{\sigma}^i_{ss'}, \quad (9)$$

where we considered only d orbitals ($l = 2$) and used $\xi^{\rm Pt}_d = 0.52$ eV, $\xi^{\rm Pd}_d = 176$ meV, and $\xi^{\rm Co}_d = 70$ meV for Pt, Pd, and Co, respectively. The values of the SOC constants ξ^I_l's were extracted from VASP-WANNIER90 non-spin-polarized calculations with SOC [41] that are in relative agreement with the previous calculations [42].

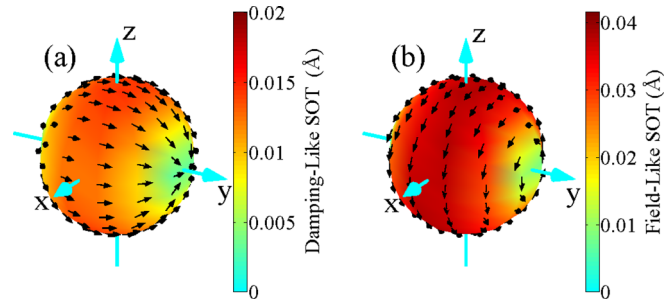

FIG. 2. Angular dependence of the total (a) DL-SOT, $\vec{\tau}^{\rm DL}_{\rm tot}$, and (b) FL-SOT, $\vec{\tau}^{\rm FL}_{\rm tot}$, on the magnetization direction $\vec{m}$ for the Pt(8 ML)/Co(6 ML) bilayer under an external electric field $\vec{E}_{\rm ext}$ along x and for the broadening parameter $\eta = 28$ meV. The color (arrow) denotes the magnitude (direction) of the SOT for each magnetization direction.

IV. RESULTS AND DISCUSSION

Figures 2(a) and 2(b) show the angular dependence of the $\vec{\tau}^{\rm DL}_{\rm tot}$ and $\vec{\tau}^{\rm FL}_{\rm tot}$ components for the Pt(8 ML)/Co(6 ML) calculated from Eqs. (4) and (6), respectively, with $\eta = 28$ meV as an example case that corresponds to a relatively clean system with room-temperature broadening. The results show that the angular dependence of the FL-SOT and DL-SOT components follow the expected $\vec{\tau}^{\rm FL} = \tau^{\rm FL}_0(\hat{y}\times\vec{m})$ and $\vec{\tau}^{\rm DL} = \tau^{\rm DL}_0\vec{m}\times(\hat{y}\times\vec{m})$ behavior, without, however, *a priori* assumption of their angular form. Within the accuracy of the calculations, we do not find any contribution from higher-order angular contributions of the magnetization direction $\vec{m}$ to the FL-SOT, as suggested by the experimental observations [8,17]. This is consistent with earlier first-principles calculations [30].

In Figs. 3(a) and 3(b) we present the FL- and DL-SOT versus the energy broadening parameter η for the Pt(8 ML)/Co(6 ML) and Pd(8 ML)/Co(6 ML) bilayer systems, using the in-plane lattice constant $a = 2.5$ Å of bulk Co. The dashed and solid curves in Fig. 3(a) represent the Fermi surface [Eq. (4)] and total [Eq. (6)] DL-SOT, respectively.

The broadening parameter η is a phenomenological parameter, which describes the effect of disorder due to impurities,

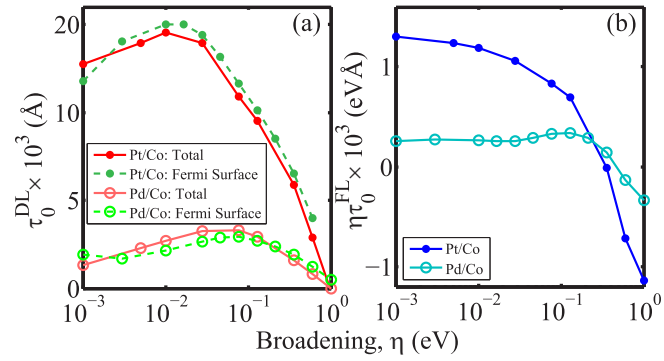

FIG. 3. (a) Fermi surface contribution (dashed curves) and total (solid curve) DL-SOT and (b) FL-SOT vs broadening parameter η for Pt(8 ML)/Co(6 ML) (solid circles) and Pd(8 ML)/Co(6 ML) (open circles) bilayers, respectively. The total and Fermi surface contributions for the DL-SOT were calculated using Eqs. (6) and (4), respectively.

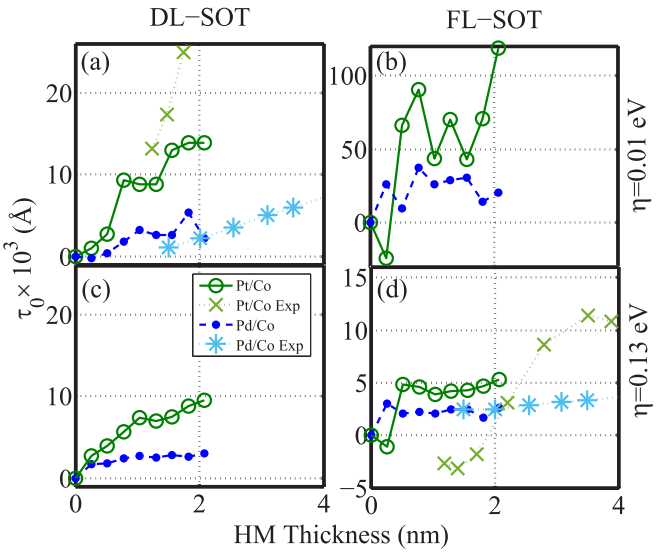

FIG. 4. Calculated DL-SOT for Pt(n ML)/Co(6 ML) (green circles) and Pd(n ML)/Co(6 ML) (blue circles) vs the HM layer thickness for η of (a) 0.01 eV (ballistic regime) and (c) 0.13 eV (diffusive regime), respectively. Calculated FL-SOT for Pt(n ML)/Co(6 ML) (green circles) and Pd(n ML)/Co(6 ML) (blue circles) vs the HM layer thickness for η of (b) 0.01 eV and (d) 0.13 eV, respectively. For comparison, we also show the experimental DL- and FL-SOT results for the Pt/Co [29] and Pd/Co [17] bilayers.

temperature, etc. It depends on the experimental growth conditions and is expected to be different for bulk versus interface local atomic environments. The results for the SOT amplitude versus η presented in Fig. 3 show that (i) within the numerical accuracy of the calculations, the DL-SOT originates exclusively from electrons on the Fermi surface, (ii) τ_0^{DL} converges to a finite value as $\eta \to 0$, while $\tau_0^{\mathrm{FL}}(\eta)$ diverges as $1/\eta$, demonstrating their intrinsic and extrinsic characteristics, respectively, and (iii) the DL-SOT exhibits a nonmonotonic dependence with η while $\eta\tau_0^{\mathrm{FL}}(\eta)$ decreases rather monotonically and changes sign for larger η values.

In order to elucidate the effect of the HM (Pt,Pd) thickness on the SOT, in Fig. 4 we display the thickness dependence of the DL- and FL-SOT for $\eta = 0.01$ eV [Figs. 4(a) and 4(b)] corresponding to a relatively clean system and $\eta = 0.13$ eV [Figs. 4(c) and 4(d)] for the "diffusive" case within the relaxation time approximation regime. The DL-SOT for the clean system [Fig. 4(a)] exhibits a nonlinear dependence on HM thickness of the form $\propto 1 - \mathrm{sech}(d_{\mathrm{HM}}/\lambda_{\mathrm{HM}}) \approx \frac{1}{2}(\frac{d_{\mathrm{HM}}}{\lambda_{\mathrm{HM}}})^2$ for small HM thickness [17]. The agreement with the experimental findings for Pd/Co [17] and Pt/Co [29] is overall good. The *ab initio* calculations underestimate the DL-SOT for Pt/Co which may be due to the strain effect shown in Fig. 5(a). On the other hand, our DL-SOT results for the Pd/Co bilayer yield a smaller spin diffusion length which may be due to the failure of the relaxation time approximation in the limit of large broadening η, where the spin diffusion length is determined by η rather than the SOC. Consequently, the treatment of systems with relatively weak SOC might require a more accurate treatment of the spin relaxation [41,43]. For the Pd/Co bilayer both the increase of the FL-SOT with increasing

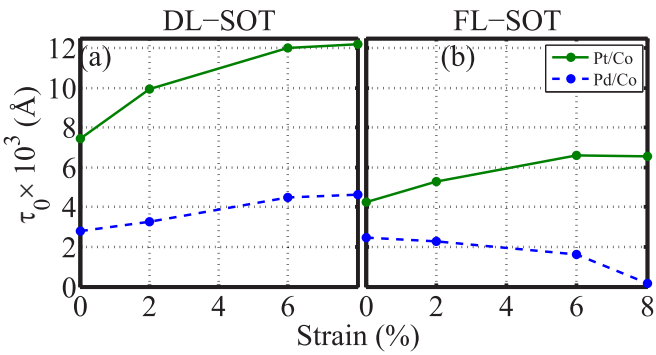

FIG. 5. (a) FL-SOT and (b) DL-SOT vs tensile biaxial in-plane strain on the Co, for Pt(6 ML)/Co(6 ML) (solid curves) and Pd(6 ML)/Co(6 ML) (dashed curves), respectively, for $\eta = 0.13$ eV.

Pd thickness and its saturation as $d_{\mathrm{Pd}} \to 0$ are consistent with experiment, indicating its interfacial origin [17]. For the Pt/Co bilayer the FL-SOT reverses sign at 1-ML Pt thickness while experiments report a reversal at about 8 ML ($\approx$2 nm) [29].

Since the lattice constants of bulk Pt ($a_{\mathrm{Pt}} = 2.8$ Å) and Pd ($a_{\mathrm{Pd}} = 2.75$ Å) are larger than that of bulk Co ($a_{\mathrm{Co}} = 2.5$ Å), in Figs. 5(a) and 5(b) we show the strain dependence of the FL- and DL-SOT, respectively, for the Pt(6 ML)/Co(6 ML) and Pd(6 ML)/Co(6 ML), where the strain $\epsilon = (a - a_{\mathrm{Co}})/a_{\mathrm{Co}}$, and the broadening parameter $\eta = 0.13$ eV, corresponding to the diffusive regime which is more pertinent to experiments on ultrathin bilayers. The increase of the DL-SOT in the Pt/Co (Pd/Co) bilayer with strain, which is relatively independent of the chosen value for η, can be attributed to the increase of the SHC, as discussed in the following.

In order to gain an insight into the origin of the SOT and how it changes with a shift of the chemical potential, e.g., due to doping, in Figs. 6(a) and 6(b) we present both the FL- and DL-SOT for the Pt(6 ML)/Co(6 ML) and Pd(6 ML)/Co(6 ML) bilayers, respectively, as a function of the Fermi level position μ-E_F (E_F is the Fermi level) for $\eta = 0.1$ eV. The FL-SOT in both systems reverses sign as the chemical potential is raised to about +0.1 eV, which may be the origin of the experimentally reported sign reversal of the FL-SOT in ultrathin Pt due to electron doping [29]. To understand the origin of the dependence of the DL-SOT on the Fermi level position in Figs. 6(c) and 6(d), we present the SHC of bulk Pt and Pd, respectively, versus the shift of the chemical potential. The SHC is calculated by replacing $\frac{1}{M_s}\vec{m}\times\frac{\partial \hat{H}_{\vec{k}}}{\partial \vec{m}}$ in Eq. (6) with $\frac{e^2}{\hbar^2 V_{\mathrm{HM}}} I_z^{S_y}$ [44],

$$\sigma_{xz}^{y} = \frac{2e^2}{\hbar^2 V_{\mathrm{HM}} N_k} \sum_{nm\vec{k}} \mathrm{Re}\left(\frac{\mathrm{Im}\left[\left(I_z^{S_y}\right)_{nm} \hat{v}_{mn}^{k_x} \right]}{(\varepsilon_{n\vec{k}} - \varepsilon_{m\vec{k}} - i\eta)^2} \right) f(\varepsilon_{n\vec{k}}), \quad (10)$$

where $I_z^{S_y} = \frac{\hbar}{4}\{\hat{\sigma}^y, \frac{\partial \hat{H}_{\vec{k}}}{\partial k_z}\}$ is the spin current operator and V_{HM} is the volume per unit cell of the bulk HM.

Due to the large in-plane lattice constant mismatch between the Pt (Pd) and Co of about -11% (-9%), we also show in Figs. 6(c) and 6(d) the SHC of the tetragonally strained bulk Pt and Pd. Our results for the bulk SHC of $2.1\times10^5(\hbar/e)(1/\Omega\,\mathrm{m})$ for Pt under zero strain in Fig. 6 is in agreement with the literature values of 1.6×10^5 [28], 2.2×10^5 [45], and 2.1×10^5 [44].

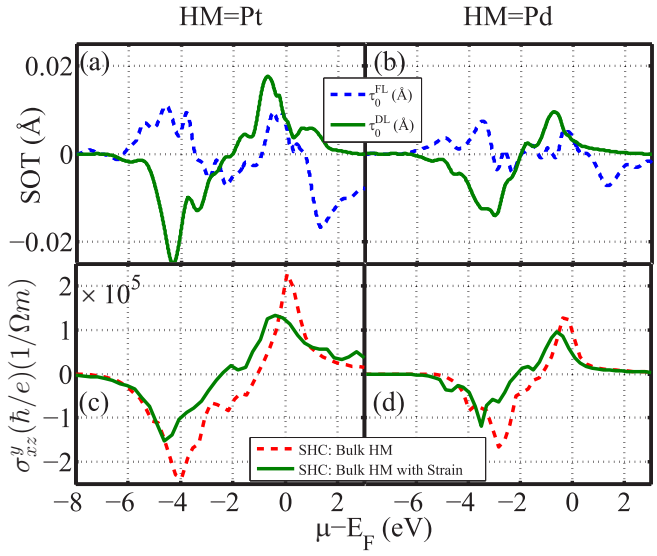

FIG. 6. FL- and DL-SOT as a function of Fermi level position for (a) Pt(6 ML)/Co(6 ML) and (b) Pd(6 ML)/Co(6 ML). Spin Hall conductivity σ_{xz}^{y} as a function of Fermi level position for bulk (c) Pt and (d) Pd. We considered both zero strain as well as −11% (−9%) compressive biaxial strain which lead to a 17% (12%) increase of the out-of-plane interlayer distance for bulk Pt (Pd).

Similarly, the bulk SHC of $1\times10^5(\hbar/e)(1/\Omega\,\mathrm{m})$, for Pd under zero strain is in good agreement with the value of 1.05×10^5 in Ref. [45].

We find that the biaxial strain results in a reduction of the maximum SHC values and a shift of the SHC peaks to lower energies. The reduction of the maximum value of the SHC with compressive biaxial strain can be understood as an interplay between the enhancement of the in-plane group velocity $\hat{v}_{mn}^{k_x}$ and the concomitant larger reduction of the out-of-plane spin current $I_z^{S_y}$ in Eq. (10), due to the increase of the in-plane and decrease of the out-of-plane hopping matrix elements, respectively. This result is also consistent with the effect of strain on the DL-SOT presented in Fig. 5(a). Figures 6(c) and 6(d) also show that the FL-SOT increases for the Pt/Co bilayer while it decreases for the Pd/Co bilayer, suggesting the absence of a universal strain dependence of the FL-SOT with biaxial tensile strain. One can clearly see the correlation of the DL-SOT with the SHC over a wide range of chemical potential shift demonstrating that the DL-SOT is dominated by the SHE of the bulk HM.

V. CONCLUDING REMARKS

We have employed an *ab initio*-based framework which links the Keldysh Green's function approach with first-principles electronic structure calculations to determine the FL- and DL-SOT of the Co/Pt and Co/Pd (111) bilayers. Without assuming *a priori* the angular form of the SOT components, we find that the dependence of the DL-SOT on magnetization direction is of the form $\vec{\tau}_{\mathrm{DL}} = \tau_0^{\mathrm{DL}}\vec{m}\times(\vec{m}\times\vec{y})$, in agreement with experiment, while that of the FL-SOT is of the form $\vec{\tau}_{\mathrm{FL}} = \tau_0^{\mathrm{FL}}\vec{m}\times\vec{y}$, which, in contrast to experiment, does not exhibit higher-order angular terms. We show that both the FL- and DL-SOTs are dominated by electrons on the Fermi surface. In Pt/Co both components of SOT increase with increasing tensile biaxial strain on Co, while in Pd/Co only the DL-SOT increases under tensile strain. The DL-SOT decreases quadratically with the HM thickness while the FL-SOT saturates to a finite value in Pt/Co while it reverses sign in Pd/Co. The dependence of the SOT with the position of the Fermi level suggests that the DL-SOT results from the spin Hall effect of the bulk HM.

ACKNOWLEDGMENTS

The work is supported by NSF ERC-Translational Applications of Nanoscale Multiferroic Systems (TANMS) Grant No. 1160504 and by NSF-Partnership in Research and Education in Materials (PREM) Grant No. DMR-1205734.

[1] A. Manchon and S. Zhang, Theory of nonequilibrium intrinsic spin torque in a single nanomagnet, Phys. Rev. B **78**, 212405 (2008).

[2] I. M. Miron, K. Garello, G. Gaudin, P.-J. Zermatten, M. V. Costache, S. Auffret, S. Bandiera, B. Rodmacq, A. Schuhl, and P. Gambardella, Perpendicular switching of a single ferromagnetic layer induced by in-plane current injection, Nature (London) **476**, 189 (2011).

[3] L. Liu, O. J. Lee, T. J. Gudmundsen, D. C. Ralph, and R. A. Buhrman, Current-Induced Switching of Perpendicularly Magnetized Magnetic Layers Using Spin Torque from the Spin Hall Effect, Phys. Rev. Lett. **109**, 096602 (2012).

[4] L. Liu, C.-F. Pai, Y. Li, H. W. Tseng, D. C. Ralph, and R. A. Buhrman, Spin-torque switching with the giant spin Hall effect of tantalum, Science **336**, 555 (2012).

[5] M. Cubukcu, O. Boulle, M. Drouard, K. Garello, C. O. Avci, I. M. Miron, J. Langer, B. Ocker, P. Gambardella, and G. Gaudin, Spin-orbit torque magnetization switching of a three-terminal perpendicular magnetic tunnel junction, Appl. Phys. Lett. **104**, 042406 (2014).

[6] C. Zhang, S. Fukami, H. Sato, F. Matsukura, and H. Ohno, Spin-orbit torque induced magnetization switching in nanoscale Ta/CoFeB/MgO, Appl. Phys. Lett. **107**, 012401 (2015).

[7] I. M. Miron, G. Gaudin, S. Auffret, B. Rodmacq, A. Schuhl, S. Pizzini, J. Vogel, and P. Gambardella, Current-driven spin torque induced by the Rashba effect in a ferromagnetic metal layer, Nat. Mater. **9**, 230 (2010).

[8] K. Garello, I. M. Miron, C. O. Avci, F. Freimuth, Y. Mokrousov, S. Blügel, S. Auffret, O. Boulle, G. Gaudin, and P. Gambardella, Symmetry and magnitude of spin-orbit torques in ferromagnetic heterostructures, Nat. Nanotechnol. **8**, 587 (2013).

[9] P. M. Haney, H.-W. Lee, K.-J. Lee, A. Manchon, and M. D. Stiles, Current induced torques and interfacial spin-orbit coupling: Semiclassical modeling, Phys. Rev. B **87**, 174411 (2013).

[10] K.-S. Lee, D. Go, A. Manchon, P. M. Haney, M. D. Stiles, H.-W. Lee, and K.-J. Lee, Angular dependence of spin-orbit spin-transfer torques, Phys. Rev. B **91**, 144401 (2015).

[11] F. Freimuth, S. Blügel, and Y. Mokrousov, Spin-orbit torques in Co/Pt(111) and Mn/W(001) magnetic bilayers from first principles, Phys. Rev. B **90**, 174423 (2014).

[12] W. Zhang, M. B. Jungfleisch, F. Freimuth, W. Jiang, J. Sklenar, J. E. Pearson, J. B. Ketterson, Y. Mokrousov, and A. Hoffmann, All-electrical manipulation of magnetization dynamics in a ferromagnet by antiferromagnets with anisotropic spin Hall effects, Phys. Rev. B **92**, 144405 (2015).

[13] S. Mondal, S. Choudhury, N. Jha, A. Ganguly, J. Sinha, and A. Barman, All-optical detection of the spin Hall angle in W/CoFeB/SiO_2 heterostructures with varying thickness of the tungsten layer, Phys. Rev. B **96**, 054414 (2017).

[14] K. Ando, S. Takahashi, K. Harii, K. Sasage, J. Ieda, S. Maekawa, and E. Saitoh, Electric Manipulation of Spin Relaxation Using the Spin Hall Effect, Phys. Rev. Lett. **101**, 036601 (2008).

[15] U. H. Pi, K. W. Kim, J. Y. Bae, S. C. Lee, Y. J. Cho, K. S. Kim, and S. Seo, Tilting of the spin orientation induced by Rashba effect in ferromagnetic metal layer, Appl. Phys. Lett. **97**, 162507 (2010).

[16] M. Hayashi, J. Kim, M. Yamanouchi, and H. Ohno, Quantitative characterization of the spin-orbit torque using harmonic Hall voltage measurements, Phys. Rev. B **89**, 144425 (2014).

[17] A. Ghosh, K. Garello, C. O. Avci, M. Gabureac, and P. Gambardella, Interface-Enhanced Spin-Orbit Torques and Current-Induced Magnetization Switching of Pd/Co/AlO_x Layers, Phys. Rev. Appl. **7**, 014004 (2017).

[18] D. MacNeill, G. M. Stiehl, M. H. D. Guimaraes, N. D. Reynolds, R. A. Buhrman, and D. C. Ralph, Thickness dependence of spin-orbit torques generated by WTe_2, Phys. Rev. B **96**, 054450 (2017).

[19] L. Liu, T. Moriyama, D. C. Ralph, and R. A. Buhrman, Spin-Torque Ferromagnetic Resonance Induced by the Spin Hall Effect, Phys. Rev. Lett. **106**, 036601 (2011).

[20] A. Kumar, S. Akansel, H. Stopfel, M. Fazlali, J. Åkerman, R. Brucas, and P. Svedlindh, Spin transfer torque ferromagnetic resonance induced spin pumping in the Fe/Pd bilayer system, Phys. Rev. B **95**, 064406 (2017).

[21] A. R. Mellnik, J. S. Lee, A. Richardella, J. L. Grab, P. J. Mintun, M. H. Fischer, A. Vaezi, A. Manchon, E.-A. Kim, N. Samarth, and D. C. Ralph, Spin-transfer torque generated by a topological insulator, Nature (London) **511**, 449 (2014).

[22] A. M. Gonçalves, I. Barsukov, Y.-J. Chen, L. Yang, J. A. Katine, and I. N. Krivorotov, Spin torque ferromagnetic resonance with magnetic field modulation, Appl. Phys. Lett. **103**, 172406 (2013).

[23] X. Fan, H. Celik, J. Wu, C. Ni, K.-J. Lee, V. O. Lorenz, and J. Q. Xiao, Quantifying interface and bulk contributions to spin-orbit torque in magnetic bilayers, Nat. Commun. **5**, 3042 (2014).

[24] X. Fan, A. R. Mellnik, W. Wang, N. Reynolds, T. Wang, H. Celik, V. O. Lorenz, D. C. Ralph, and J. Q. Xiao, All-optical vector measurement of spin-orbit-induced torques using both polar and quadratic magneto-optic Kerr effects, Appl. Phys. Lett. **109**, 122406 (2016).

[25] X. Qiu, P. Deorani, K. Narayanapillai, K.-S. Lee, K.-J. Lee, H.-W. Lee, and Hyunsoo Yang, Angular and temperature dependence of current induced spin-orbit effective fields in Ta/CoFeB/MgO nanowires, Sci. Rep. **4**, 4491 (2014).

[26] J. Kim, J. Sinha, M. Hayashi, M. Yamanouchi, S. Fukami, T. Suzuki, S. Mitani, and H. Ohno, Layer thickness dependence of the current-induced effective field vector in Ta|CoFeB|MgO, Nat. Mater. **12**, 240 (2013).

[27] F. Mahfouzi, B. K. Nikolić, and N. Kioussis, Antidamping spin-orbit torque driven by spin-flip reflection mechanism on the surface of a topological insulator: A time-dependent nonequilibrium Green function approach, Phys. Rev. B **93**, 115419 (2016).

[28] L. Wang, R. J. H. Wesselink, Y. Liu, Z. Yuan, K. Xia, and P. J. Kelly, Giant Room Temperature Interface Spin Hall and Inverse Spin Hall Effects, Phys. Rev. Lett. **116**, 196602 (2016).

[29] M.-H. Nguyen, D. C. Ralph, and R. A. Buhrman, Spin Torque Study of the Spin Hall Conductivity and Spin Diffusion Length in Platinum Thin Films with Varying Resistivity, Phys. Rev. Lett. **116**, 126601 (2016).

[30] F. S. M. Guimaraes, M. dos S. Dias, J. Bouaziz, A. T. Costa, R. B. Muniz, and S. Lounis, Dynamical amplification of magnetoresistances and Hall currents up to the THz regime, Sci. Rep. **7**, 3686 (2017).

[31] F. Mahfouzi, Nonequilibrium Green function approach to elastic and inelastic spin-charge transport in topological insulator-based heterostructures and magnetic tunnel junctions, Ph.D. dissertation, University of Delaware, 2014, http://udspace.udel.edu/handle/19716/16765.

[32] H. Kurebayashi, J. Sinova, D. Fang, A. C. Irvine, T. D. Skinner, J. Wunderlich, V. Novák, R. P. Campion, B. L. Gallagher, E. K. Vehstedt, L. P. Zârbo, K. Výborný, A. J. Ferguson, and T. Jungwirth, An antidamping spin-orbit torque originating from the Berry curvature, Nat. Nanotechnol. **9**, 211 (2014).

[33] F. Mahfouzi, B. K. Nikolić, S.-H. Chen, and C.-R. Chang, Microwave-driven ferromagnet-topological-insulator heterostructures: The prospect for giant spin battery effect and quantized charge pump devices, Phys. Rev. B **82**, 195440 (2010).

[34] S. Ghosh and A. Manchon, Spin-orbit torque in a three-dimensional topological insulator-ferromagnet heterostructure: Crossover between bulk and surface transport, Phys. Rev. B **97**, 134402 (2018).

[35] G. Kresse and J. Furthmüller, Efficient iterative schemes for ab initio total-energy calculations using a plane-wave basis set, Phys. Rev. B **54**, 11169 (1996).

[36] G. Kresse and J. Furthmüller, Efficiency of ab-initio total energy calculations for metals and semiconductors using a plane-wave basis set, Comput. Mater. Sci. **6**, 15 (1996).

[37] P. E. Blöchl, Projector augmented-wave method, Phys. Rev. B **50**, 17953 (1994).

[38] G. Kresse and D. Joubert, From ultrasoft pseudopotentials to the projector augmented-wave method, Phys. Rev. B **59**, 1758 (1999).

[39] J. P. Perdew, K. Burke, and M. Ernzerhof, Generalized Gradient Approximation Made Simple, Phys. Rev. Lett. **77**, 3865 (1996).

[40] A. A. Mostofi, J. R. Yates, G. Pizzi, Y.-S. Lee, I. Souza, D. Vanderbilt, and N. Marzari, An updated version of WANNIER90: A tool for obtaining maximally-localised Wannier functions, Comput. Phys. Commun. **185**, 2309 (2014).

[41] F. Mahfouzi, J. Kim, and N. Kioussis, Intrinsic damping phenomena from quantum to classical magnets: An ab initio study of Gilbert damping in a Pt/Co bilayer, Phys. Rev. B **96**, 214421 (2017).

[42] S. Grytsyuk, A. Belabbes, P. M. Haney, H.-W. Lee, K.-J. Lee, M. D. Stiles, U. Schwingenschlögl, and A. Manchon, *k*-asymmetric spin splitting at the interface between transition

metal ferromagnets and heavy metals, Phys. Rev. B **93**, 174421 (2016).

[43] Y. Liu, Z. Yuan, R. J. H. Wesselink, A. A. Starikov, M. van Schilfgaarde, and P. J. Kelly, Direct method for calculating temperature-dependent transport properties, Phys. Rev. B **91**, 220405(R) (2015).

[44] G. Y. Guo, S. Murakami, T.-W. Chen, and N. Nagaosa, Intrinsic Spin Hall Effect in Platinum: First-Principles Calculations, Phys. Rev. Lett. **100**, 096401 (2008).

[45] W. Zhang, M. B. Jungfleisch, W. Jiang, Y. Liu, J. E. Pearson, S. G. E. te Velthuis, and A. Hoffmann, Reduced spin-Hall effects from magnetic proximity, Phys. Rev. B **91**, 115316 (2015).